Lecture Notes in Electrical Engineering 755

Abhijit Biswas
Raghvendra Saxena
Debashis De *Editors*

Microelectronics, Circuits and Systems

Select Proceedings of 7th International Conference on Micro2020

Springer

Unified Analytical Model for Charge Density and Plasmonic Waves in the Quaternary AlInGaN/AlN/GaN Heterostructures

Manju K. Chattopadhyay and Kavita Thorat Upadhyay

1 Introduction

Lately, the Terahertz (THz) sources are gaining attention due to their possible applications in spectroscopy, bio-medical imaging, and high-speed communication. Traditionally accessible terahertz suppliers included vacuum devices and cryogenic QCLs [1]. However, these devices were bulky, besides being unstable at room temperature THz signal generation.

Dyakonov and Shur theoretically envisaged that solid-state field-effect transistors could find applications as THz detectors for both resonant and non-resonant THz waves [2]. Their theory paved way for wide research on the new concept of traveling wave transistor. Various kinds of THz detectors based on solid-state devices viz. the Si metal–oxide–semiconductor field-effect transistors (MOSFETs), high electron mobility transistors (HEMTs)), and graphene FETs have been widely researched [3, 4].

As compared to the Si MOSFET, wurtzite AlGaN/GaN MODFET has superior carrier mobility and higher two-dimensional electron gas (2DEG) density, owing to the spontaneous and piezoelectric polarization effects. These effects lead to elevated responsivity and low noise equivalent power (NEP) at ambient temperature. Additionally, the manufacturing procedure is less complex as the 2DEG heterointerface is formed by spontaneous polarization without any deliberate doping. Because of these advantages, the AlGaN/GaN heterostructures are considered promising as THz detectors. Knap et al. reported an AlGaN/GaN HEMT-based THz detector with the

M. K. Chattopadhyay (✉)
School of Electronics, Devi Ahilya University, Khandwa Road, Indore 452017, MP, India

K. T. Upadhyay
Department of Electronics and Communication Engineering, IPS Academy, Institute of Engineering and Science, Indore 452012, MP, India

Department of Electronics and Telecommunication Engineering, Institute of Engineering and Technology, Devi Ahilya University, Indore 452017, MP, India

A. Biswas et al. (eds.), *Microelectronics, Circuits and Systems*, Lecture Notes in Electrical Engineering 755, https://doi.org/10.1007/978-981-16-1570-2_16

detectable frequency in the 100–600 GHz range [5]. Sun et al. demonstrated THz detection by a floating antenna-based AlGaN/GaN HEMT with elevated responsivity R_v of (3.6 kV/W) and a small NEP (40 pW/Hz$^{0.5}$) at room temperature [6]. Hou et al. also proposed a GaN HEMT with the highest R_v of 15 kV/W and the smallest value of 0.58 pW/Hz$^{0.5}$ as NEP with 0.25 μm gate length [7]. Traditionally, the AlGaN barrier layer has a constraint of the critical thickness of at least 10 nm to supply adequate 2DEG concentration. This limit blocks the frequency performance enhancement. To facilitate the increase in device frequency and to have a higher charge concentration, a thinner barrier layer is required.

The quaternary alloy semiconductor $Al_xIn_yGa_{1-x-y}N$ has clear advantages over the ternary AlGaN material. Firstly, the bandgap and lattice constants can be engineered individually, resulting in reduced defects, misfit locations, cracks, and piezoelectric field. This also allows the development of a skeletal Schottky barrier layer without significant immiscibility-associated problems in AlN, In, and GaN [8]. Secondly, with higher *Al* content, larger polarization strength can be realized because of increased spontaneous polarization in $Al_xIn_yGa_{1-x-y}N$. By using proper In and Al compositions, high 2DEG concentration in $Al_xIn_yGa_{1-x-y}N$ structures can be attained even using a thin barrier layer with better controllability by the gate voltage. Therefore, the solid-state heterostructures, consisting of a GaN channel and an AlInGaN barrier layer, are considered promising for high-power THz applications.

We propose a THz device based on AlInGaN/AlN/GaN HEMT in the present work. We present a unified analytical model for sheet charge density and plasmonic waves in quaternary AlInGaN/AlN/GaN HEMTs. This sheet charge density is used in expressions to calculate the directly proportional Plasmon frequency. Section 2 below describes our 2DEG charge density *(n_s)* model. Expressions for Plasmon frequency and other parameters used are given in the Sect. 2 too. Results are discussed in Sect. 3, and the present work is concluded in Sect. 4 (Figs. 1 and 2).

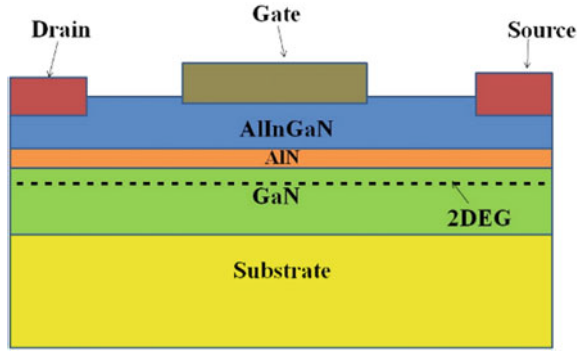

Fig. 1 Cross-sectional diagram of quaternary AlInGaN/GaN HEMT structure

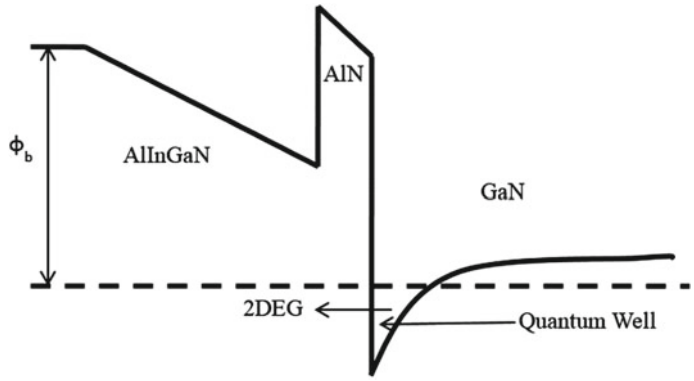

Fig. 2 Energy band diagram of the device

2 Calculations for 2DEG Charge Model

2.1 Polarization Calculations for the AlInGaN/AlN/GaN HEMT

Configuration of the 2DEG is a pertinent use of the polarization characteristics of the nitride alloy. In the literature, a good amount of valuable predictions on the polarization property of the ternary alloys is available. However, little work in literature is available with a special focus on the polarization property of quaternary AlInGaN alloy.

Structural and electronics properties can be attained by linearly interpolating the formulae based on Vegard's law. On the other hand, many structural parameters and the energy bandgap are non-linear. Therefore, in our model, we use bowing-based interpolation formulae. The bowing model requires non-linear data of applicable quantities only at the same portions of compositions [9]. In the case of the AlInGaN/GaN HEMTs, the polarization-dependent threshold voltage is given as

$$V_{th} = \varnothing_b - \Delta E_c - q N_d d_d^2/2\varepsilon - \sigma_{int}(d_d)/\varepsilon \tag{1}$$

where $\varnothing_b$ is the Schottky barrier height, ΔE_c is the conduction band discontinuity, N_d is the doping concentration, ε is the permittivity of AlInGaN, and d_d is the thickness of the AlInGaN layer,

$$\sigma_{int} = P_{GaN} - P_{AlInGaN} \tag{2}$$

and

$$P_{AlInGaN} = P_{sp}(AlInGaN) + P_{pz}(AlInGaN) \tag{3}$$

i.e., Sum of spontaneous and piezoelectric polarization.

For a practical AlInGaN/GaN heterostructure, a thin AlN layer, usually of 1 nm width, is introduced at the heterojunction to reduce the alloy disorder scattering from the AlInGaN barrier layer and to increase the charge density. We estimate its outcome by substituting the conduction band offset ΔE_c in Eq. (1) by our modified conduction band offset as

$$\Delta E_{c\_mod} = \Delta E_{c\_AlN/GaN} - \Delta E_{c\_AlInGaN/AlN} + \Delta E_{c\_AlN} \tag{4}$$

Here, we have taken

$$\Delta E_{c\_AlN} = \frac{q^2 d_{AlN}}{\varepsilon_{AlN}}\left(\frac{\sigma_{AlN}}{q} - n_s\right) \tag{5}$$

Various other terms are as defined in Table 1.

2.2 Carrier Density Model

The sheet charge density n_s can be obtained by solving the 1D Poisson's equation and can be represented as

$$n_s = \varepsilon\big(V_g - V_{th} - V_k - E_F/q\big)/q\mathrm{d} \tag{6}$$

where d is the sum of d_d and the length of the AlN layer, V_k is the channel voltage at distance k, and E_F is the Fermi level.

An analytical expression for n_s as a function of V_g can be expressed as [10]

$$n_s = \big[AV_{go}/(1+B)\big]\big[\big(1 - A^{2/3}\gamma_0\big)/(1+B)^{2/3}V_{go}^{1/3}\big] \tag{7}$$

$A = \varepsilon/qd$ and $B = A/qD$, and D is the two-dimensional density of states inside the quantum well at the heterointerface.

The unified expression for n_s including the contribution of charge carriers in the barrier layer is given as [11]

$$n_{s,unified} = \frac{2k_BTA\ln\left(1 + exp^{\left(\frac{qV_{go}}{2k_BT}\right)}\right)}{q\left(\frac{AV_{go}}{n_{s,AboveVth}} + \frac{A}{D}exp^{\left(\frac{-qV_{go}}{2k_BT}\right)}\right)} \tag{8}$$

here $V_{go} = V_g - V_{th}$.

Table 1 Material specific parameters for the calculations

Parameters	Values/Details
Polarization charge across the AlN/GaN interface	σ_{AlN}
Thickness of the AlN layer	d_{AlN}
Conduction band offset at the AlN/GaN interface	$\Delta E_{c\_AlN/GaN}$
Conduction band offset at the AlInGaN/GaN interface	$\Delta E_{c\_AlInGaN/AlN}$
Permittivity of the AlN layer	ε_{AlN}
Spontaneous polarization	$P_{sp}(AlInGaN) = x \cdot P_{sp}(AlN) + y \cdot P_{sp}(InN) + z \cdot P_{sp}(GaN) + b_{AlGaN} \cdot z \cdot + b_{InGaN} \cdot y \cdot z + b_{AlInN} \cdot x \cdot y + b_{AlInGaN} \cdot x \cdot y \cdot z$
$b_{AlGaN}, b_{InGaN}, b_{AlInN}$ are bowing parameters of ternary alloy	$b_{AlInGaN} = 27P_{sp}(Al_{0.33}In_{0.33}Ga_{0.33}N) - 9(b_{AlGaN} + b_{InGaN} + b_{AlInN}) - 3(P_{sp}(AlN) + P_{sp}(InN) + P_{sp}(GaN))$
Basal strain defined after Vegard's interpolation of lattice parameter	$\eta\left(U_x V_y Ga_z N\right) = \frac{[x(a^{GaN} - a^{UN}) + y(a^{GaN} - a^{VN})]}{[xa^{UN} + ya^{VN} + za^{GaN}]}$
Piezoelectric polarization parameters	$P_{pz}(AlInGaN) = x \cdot P_{pz}(AlN, \eta) + y \cdot P_{pz}(InN, \eta) + z \cdot P_{pz}(GaN, \eta)$ $P_{pz}(AlN, \eta) = -1.808\eta + 5.624\eta^2 for \eta < 0$ $P_{pz}(AlN, \eta) = -1.808\eta - 7.888\eta^2 for \eta > 0$ $P_{pz}(GaN, \eta) = -0.918\eta + 9.541\eta^2$ $P_{pz}(InN, \eta) = -1.373\eta + 7.559\eta^2$
Energy bandgap	$E_g(GaN) = 3.4\text{eV}, E_g(AlN) = 6.2\text{eV}, E_g(InN) = 0.7eV$

2.3 Model for Drain Current

The model for drain current may be formulated by calculating the current along the channel.

$$I_d = q\mu_0 W n_{s,unified} v_s \tag{9}$$

where μ_0 is the low vertical field mobility, W is the width of the device, and v_s is the drift velocity.

Integrating from source to drain gives a simple analytical model of the drain current as

$$I_d = \left(\frac{q\mu_{eff}W}{L_g}\right)\left\{\left[\frac{(A+D)\left(n_s^2 - n_D^2\right)}{2AD}\right] + \left(\frac{2}{5}\gamma_0\left(n_s^{5/3} - n_D^{5/3}\right)\right) + \frac{k_B T(n_s - n_D)}{q}\right\} \quad (10)$$

where n_s and n_D are the electron charge densities at the source and drain ends, respectively, L_g is the gate length, and the rest of the symbols are defined as done conventionally. The calculations of n_D and saturation voltage V_{sat} are given in our previous work [10].

The second-order effects such as drain-induced barrier lowering (DIBL), channel length modulation, and self-heating effects (SHE) are neglected here but can be included in I_d–V_d characteristics by modifying the Eq. (4), in a procedure similar to our earlier work [12].

2.4 Dispersion Relations for Plasma Waves in 2D Gated Devices

In two- or one-dimensional plasma, the frequency of plasma oscillations, ω_p depends on the plasma wave vector k. Theoretical modeling of a 2D plasma leads to the following dispersion relationship [13]:

$$\omega_p = \sqrt{\frac{q^2 n_s k}{2m^* \varepsilon_0 \varepsilon_{GaN}}}, k = \sqrt{\frac{qV_{go}}{m^*}} k_n \text{ for } kd \ll 1$$

$$(k_n)_{gated} = \frac{(2n-1)\pi}{L_g}, \text{ where } n = 1, 2, 3 \ldots$$

The plasma waves propagate with much greater velocities than the electron drift velocities. Hence, the plasma wave frequency for the fundamental harmonic for short-channel solid-state devices is in the THz range. Other relations used for various parameters related to plasmon oscillations are listed in Table 2.

Table 2 Relationship used for various parameters related to plasmon oscillations

Parameter with units	Relationship
Characteristic length for the ac voltage decay from the source [15]	$L_o = s\sqrt{\tau/m}$
Electron effective mass in AlInGaN layer	$m^* = (0.35x + 0.1y + 0.2z)m_0$
Fermi velocity [16]	$v_F = \frac{h}{2\pi}\frac{1}{m^*}\sqrt{2\pi n_s}$
Electron plasma velocity [16]	$S = \sqrt{\frac{q^2 n_s d}{\epsilon m^*}}$
Fundamental plasma frequency [16]	$f = \frac{S}{4L_g}$

Plasma wave electronic devices have a major benefit that they can be tuned by applying bias voltage and are able to modulate at very high frequencies viz. 200 GHz and more [14]. This makes quaternary GaN heterostructures interesting devices for probable employability in high-power, ultrahigh-speed wireless communications used in the ultrahigh-resolution broadcast.

3 Results and Discussion

Figure 3 shows the comparison of our calculated output characteristics and experimental data published by Hwang et al. [8]. Values of various parameters used are given in Table 3. High drain currents of 1589 A/mm, 1278 A/mm, 865 A/mm, and

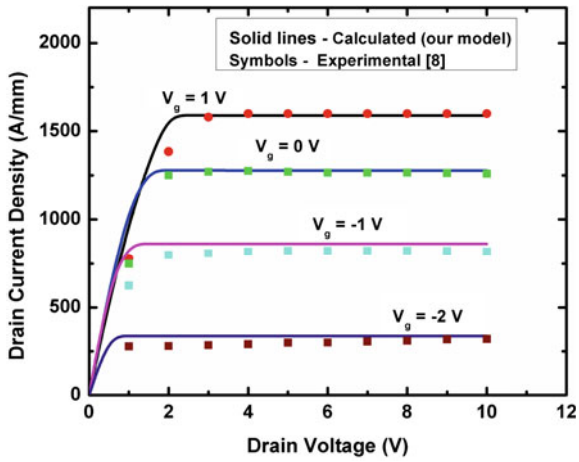

Fig. 3 I_d–V_d characteristics of heterostructure at different gate voltages V_g

Table 3 Model and device parameters used in calculations for comparison in figure

Parameter with units		Values employed in our computations
L_g (μm)		400 nm
W (μm)		1 μm
μ_0 (cm^2/V-s)		1621
Fitting parameters	a_1 (1/V)	-40×10^{-3}
	a_2 (1/V^2)	0.32
	a_3(1/V)	5×10^{-5}
Transition width parameter	α, (unit less)	1.2
R_s (Ω)		0.6
R_d (Ω)		0.6

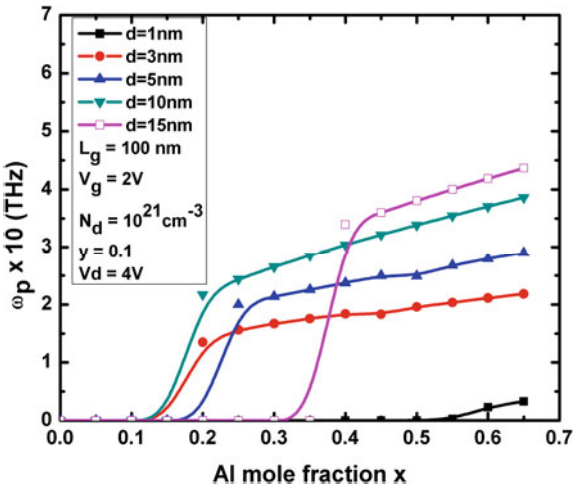

Fig. 4 Plasma frequency ω_p versus *Al* mole fraction *x*

337 A/mm are obtained at gate voltages 1 V, 0 V, −1 V, and −2 V, respectively. By choosing suitable fitting parameters, we obtained a good match with the experimental result.

The relationship of plasma frequency ω_p with *x,* the *Al* mole fraction, is depicted in Fig. 4 for $L_g = 100$ nm. A higher frequency range is observed for higher values of *d*. The frequencies observed are higher by an order as compared to calculations done for AlGaN/GaN HEMTs by Rabbaa et al. [17]. ω_p achieved values more than 40 THz for $d = 15$ nm and $L_g = 100$ nm.

Figure 5 illustrates the variation of plasma frequency ω_p with doping density at different gate voltages applied. A linear relationship of ω_p is seen with the doping

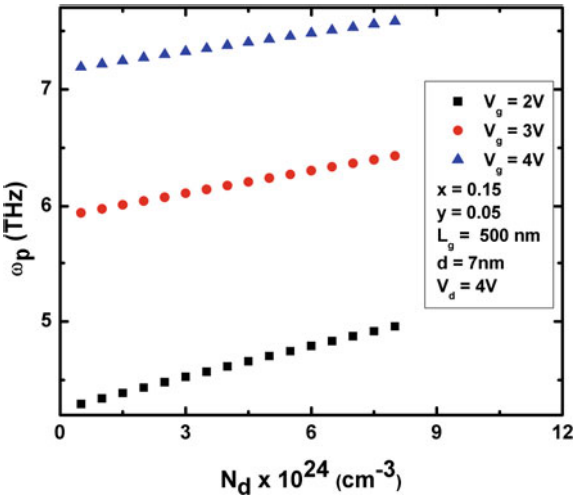

Fig. 5 Plasma frequency versus doping density for different gate voltages V_g

density N_d and the V_g. The relationship of Plasma and Fermi velocities with 2DEG is shown in Fig. 6. We infer that the plasma wave velocity reaches a much higher value of 27.6×10^5 m/s as compared to the Fermi velocity of 9.4×10^5 m/s for a sheet charge concentration of 10^{17} cm^{-3}.

Change in calculated plasma frequency ω_p versus V_g for different *In* mole fractions y is illustrated in Fig. 7 with *Al* mole fraction x fixed at 0.3. It is observed that the lower y values give higher plasma frequencies. Figure 8 depicts the variation of fundamental plasma frequency f with the gate length L_g at a drain voltage of 4 V for gate voltages from 2 to 5 V. We see that f rises exponentially with a decrease in L_g. Although we attain great THz plasmon frequencies by lessening the L_g, there are certain limitations

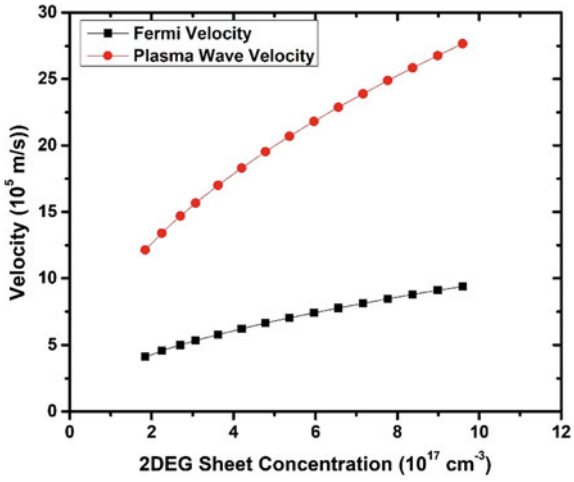

Fig. 6 Plasma velocity S and Fermi velocity v_F versus 2DEG sheet concentration

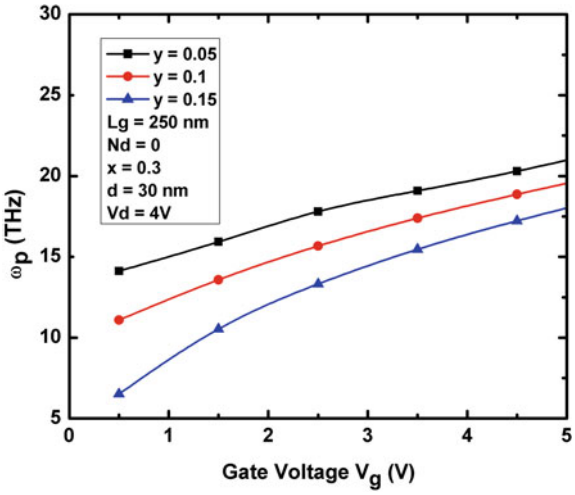

Fig. 7 Calculated plasma frequency ω_p versus gate voltage for different Indium mole fractions y

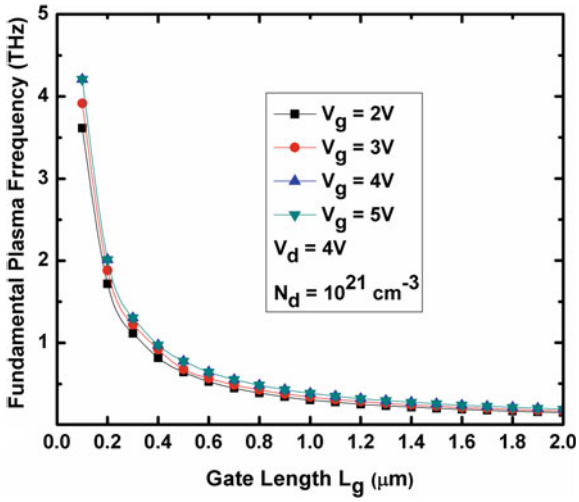

Fig. 8 Fundamental plasma frequency f versus gate length L_g for various gate voltages

with very short gate lengths while designing the HEMTs. Therefore, one has to ascertain the minimum critical gate length for optimized operation.

4 Conclusion

A unified analytical model for calculating sheet charge density and plasma frequency of Terahertz waves in quaternary AlInGaN/AlN/GaN HEMTs is presented. Calculated results using our model matched well for I_d–V_d characteristics of experimental data given in Ref. [8]. We observed that due to higher electron concentration accumulation in quaternary alloys as compared to ternary alloys such as AlGaN, the plasmon oscillations introduced have higher frequency by almost an order. Our unified analytical model gives an overview of different parameter relationships for exploring the quaternary alloy-based HEMTs for THz device applications.

References

1. Dunn, A., Poyser, C., Dean, P., Demić, A., Valavanis, A., Indjin, D., Salih, M., Kundu, I., Li, L., Akimov, A., Davies, A.G.: High-speed modulation of a terahertz quantum cascade laser by coherent acoustic phonon pulses. Nat. Commun. **11**(1), 1–8 (2020)
2. Dyakonov, M.I., Shur, M.S.: Detection, mixing, and frequency multiplication of terahertz radiation by two-dimensional electronic fluid. IEEE Trans. Electron Dev. **43**(10), 380–387 (1996)
3. Ahi, K.: Review of GaN-based devices for terahertz operation. Opt. Eng. **56**(9), 090901 (2017)
4. Božanić, M., Sinha, S.: Emerging transistor technologies capable of terahertz amplification: a way to re-engineer terahertz radar sensors. Sensors **19**(11), 2454 (2019)

5. Knap, W., Dyakonov, M., Coquillat, D., Teppe, F., Dyakonova, N., Łusakowski, J., Karpierz, K., Sakowicz, M., Valusis, G., Seliuta, D., Kasalynas, I.: Field effect transistors for terahertz detection: physics and first imaging applications. J. Infrared Millim. Terahertz Waves **30**(12), 1319–1337 (2009)
6. Sun, J.D., Sun, Y.F., Wu, D.M., Cai, Y., Qin, H., Zhang, B.S.: High-responsivity, low-noise, room-temperature, self-mixing terahertz detector realized using floating antennas on a GaN-based field-effect transistor. Appl. Phys. Lett. **100**(1), 013506 (2012)
7. Hou, H., Liu, Z., Teng, J., Palacios, T., Chua, S.J.: A sub-terahertz broadband detector based on a GaN high-electron-mobility transistor with nanoantennas. Appl. Phys. Express **10**(1), 014101 (2016)
8. Hwang, J.H., Kim, S.M., Woo, J.M., Hong, S.M., Jang, J.H.: GaN HEMTs with quaternary In0. 05Al0. 75Ga0. 2N Schottky barrier layer. Physica Status Solidi A **213**(4), 889–892 (2016)
9. Fiorentini, V., Bernardini, F., Ambacher, O.: Evidence for nonlinear macroscopic polarization in III–V nitride alloy heterostructures. Appl. Phys. Lett. **80**(7), 1204–1206 (2002)
10. Upadhyay, K.T., Chattopadhyay, M.K.: Al composition and $Al_xIn_yGa_zN$ layer thickness dependent new analytical model for I-V characteristics of $Al_xIn_yGa_zN$/GaN HEMTs. **19**(2), 205–208 (2019)
11. Swamy, N.S., Dutta, A.K.: Analytical models for the 2DEG density, AlGaN layer carrier density, and drain current for AlGaN/GaN HEMTs. IEEE Trans. Electron. Dev. **65**(3), 936–944 (2018)
12. Chattopadhyay, M.K., Tokekar, S.: Thermal model for dc characteristics of ALGaN/GaN hemts including self-heating effect and non-linear polarization. Microelectron. J. **39**(10), 1181–1188 (2008)
13. Stern, F.: Polarizability of a two-dimensional electron gas. Phys. Rev. Lett. **18**(14), 546 (1967)
14. Otsuji, T., Shur, M.: Terahertz plasmonics: good results and great expectations. IEEE Microwave Mag. **15**(7), 43–50 (2017)
15. Liu, Shur, M.: An efficient TCAD model for TeraFET detectors. In: IEEE Radio and Wireless Symposium (RWS) (2019)
16. Shur, M.: AlGaN/GaN plasmonic terahertz electronic devices. J. Phys. Conf. Ser. **486**, 012025 (2014)
17. Rabbaa, S., Stiens, J.: Charge density and plasmon modes in a triangular quantum well model for doped and undoped gated AlGaN/GaN HEMTs. J. Phys. D Appl. Phys. **44**, 32 (2011)